

## The Northwest Africa (NWA) 5790 meteorite: A mesostasis-rich nakhlite with little or no Martian aqueous alteration

Tim TOMKINSON<sup>1\*</sup>, Martin R. LEE<sup>2</sup>, Darren F. MARK<sup>1</sup>, Katherine J. DOBSON<sup>3,4</sup>,  
and Ian A. FRANCHI<sup>5</sup>

<sup>1</sup>Scottish Universities Environmental Research Centre, Scottish Enterprise Technology Park, Rankine Avenue, East Kilbride G75 0QF, UK

<sup>2</sup>School of Geographical and Earth Sciences, University of Glasgow, Gregory Building, Lilybank Gardens, Glasgow G12 8QQ, UK

<sup>3</sup>Manchester X-ray Imaging Facility, School of Materials, The University of Manchester, Oxford Road, Manchester M13 9PL, UK

<sup>4</sup>Rutherford Appleton Laboratories, Research Complex at Harwell, Didcot, Oxfordshire OX11 0FA, UK

<sup>5</sup>Department of Physical Sciences, The Open University, Walton Hall, Milton Keynes MK7 6AA, UK

\*Corresponding author. E-mail: tim.tomkinson@glasgow.ac.uk

(Received 20 March 2014; revision accepted 06 December 2014)

**Abstract**—Northwest Africa (NWA) 5790 is the most recently discovered member of the nakhlite group. Its mineralogy differs from the other nakhlites with a high abundance mesostasis ( $38.1 \pm 3.6$  vol%) and scarcity of olivine ( $4.0 \pm 2.2$  vol%). Furthermore, zoning of augite phenocrysts, and other petrographic and chemical characteristics suggest that NWA 5790 samples the chilled margin of its parent lava flow/sill. NWA 5790 contains calcite and rare clay minerals that are evidence for its exposure to liquid water. The calcite forms a cement to coatings of dust on the outer surface of the find and extends into the interior of the meteorite within veins. The presence of microbial remains within the coating confirms that the dust and its carbonate cement are terrestrial in origin, consistent with the carbon and oxygen isotope composition of the calcite. The clay minerals are finely crystalline and comprise  $\sim 0.003$  vol% of the meteorite.  $\delta D$  values of the clay minerals range from  $-212 \pm 109\text{‰}$  to  $-96 \pm 132\text{‰}$ , and cannot be used to distinguish between a terrestrial or Martian origin. As petrographic results are also not definitive, we conclude that secondary minerals produced by Martian groundwaters are at best very rare within NWA 5790. The meteorite has therefore sampled a region of the lava flow/sill with little or no exposure to the aqueous solutions that altered other nakhlites. This isolation could relate to the scarcity of olivine in NWA 5790 because dissolution of olivine in other nakhlites by Martian groundwaters enhanced their porosity and permeability, and provided solutes for secondary minerals.

### INTRODUCTION

The meteorites Allan Hills (ALH) 84001, NWA 7034 (paired with NWA 7533), and the SNC clan (shergottites, nakhlites, and chassignites) are samples of the crust of Mars, and together provide unique insights into the planet's evolution (e.g., Treiman et al. 2000; Treiman 2005; McSween et al. 2009; Basu Sarbadhikari et al. 2011; Agee et al. 2013; Humayun et al. 2013; Cartwright et al. 2014). Members of the nakhlite group

are distinct from other Martian meteorites with respect to their crystallization age ( $\sim 1.3$  Ga; Nyquist et al. 2001), moderate levels of shock (2–25 GPa; Fritz et al. 2005), and mineralogy (clinopyroxenites with varying abundances of olivine, titanomagnetite, a feldspar-rich or glassy mesostasis, and secondary minerals formed from Martian water; Treiman 2005). NWA 5790 was recovered from the Sahara desert in 2009, and shortly thereafter recognized as the eighth nakhlite (Jambon et al. 2010; Weisberg et al. 2010); it is possibly paired

Table 1. Modal mineralogy of NWA 5790 (vol%).

	Area (mm <sup>2</sup> )	Augite	Mesostasis	Olivine	Titanomagnetite
XCT slice 500	65.4	59.1	35.5	4.4	1
XCT slice 600	97.4	57.4	36	5.6	1
XCT slice 700	109.1	61.3	34.7	2.8	1.2
XCT slice 800	125.2	53.1	44.2	2	0.7
XCT slice 900	123.1	54.1	41.5	3.7	0.7
XCT slice 1000	103.8	59.5	37.3	2.7	0.8
Polished block mean	45.5	58.9	36.1	3.8	1.1
Standard deviation (1 $\sigma$ )		2.5	1.6	0.9	0.1
Jambon et al. (2010) and Weisberg et al. (2010)		51.2	39.7	9.1	<1
Mikouchi et al. (2012)		—	33.6	—	—
Corrigan et al. (2014)		56 $\pm$ 2	42 $\pm$ 0.1	$\sim$ 2 $\pm$ 0.4	<1
Overall mean		56.7	38.1	4	0.9
Standard deviation (1 $\sigma$ )		3.4	3.6	2.2	0.2

— denotes not stated. The polished block data are means of three point counts across the same sample in different orientations ( $n = 384, 416,$  and 417 points).

with NWA 6148 (Corrigan et al. 2014). Its ages of crystallization ( $1.38 \pm 0.07$  Ga; Shih et al. 2010) and ejection ( $\sim 9.6$  Ma; Huber et al. 2012) are consistent with those of the other seven members of the group: Governador Valadares, Lafayette, Miller Range (MIL) 03346 (paired with MIL 090030, 090032, 090036), Nakhla, NWA 817, NWA 998, and Yamato (Y-) 000593 (paired with Y-000749 and -000802).

Models of nakhlite petrogenesis suggest that they crystallized within a common lava flow or shallow sill (e.g., Friedman-Lentz et al. 1999; Treiman 2005; Korochantseva et al. 2011), although there is a possibility that these rocks sample multiple flows/intrusions. Assuming a single lava flow/sill, the relative positions of individual meteorites within the igneous body can be estimated using differences between them in properties including (1) the abundance of the intercumulate mesostasis and its degree of crystallinity (i.e., plagioclase feldspar versus glass), (2) zoning of cumulus pyroxene and olivine grains, and (3) Al<sub>2</sub>O<sub>3</sub> content of the cores of pyroxene grains (e.g., Mikouchi et al. 2003, 2006, 2012; Treiman 2005; McKay et al. 2006). These igneous rocks also interacted with Martian aqueous solutions to form secondary minerals (including carbonates and clay minerals), but the origin of the water is unclear, as is the means by which it gained access to the igneous body. Models of nakhlite alteration range from a small scale and chemically near-closed system (Treiman et al. 1993; Treiman and Lindstrom 1997; Grady et al. 2007; Lee et al. 2013; Tomkinson et al. 2013) to a large-scale impact-induced hydrothermal cell (Changela and Bridges 2011).

As the most recent nakhlite find, NWA 5790 presents an opportunity to test the models of nakhlite crystallization and aqueous alteration. Several studies have described its mineralogy, mineral chemistry, and

bulk chemical and isotopic composition (Jambon et al. 2010; Shih et al. 2010; Weisberg et al. 2010; Sanborn et al. 2011; Mikouchi et al. 2012; Corrigan et al. 2013, 2014; McCubbin et al. 2013). Results from this work show that NWA 5790 differs from the other nakhlites in two important respects. First, it has several characteristics, including a relatively high volume of mesostasis and strongly zoned augite phenocrysts, which suggest that it crystallized at the chilled margin of the igneous body, and possibly in its upper edge (Jambon et al. 2010; Mikouchi et al. 2012). However, there are substantial differences between previous determinations of modal mineralogy, with values for mesostasis abundance ranging from 33.6 vol% (Mikouchi et al. 2012) to 42.0 vol% (Corrigan et al. 2014) (Table 1). Thus, one goal of the present study was to re-examine one of the key properties of NWA 5790 that has been used to locate it relative to the other nakhlites in a Martian igneous complex. We have done this by accurately quantifying the modal mineralogy of a bulk sample using X-ray computed tomography (XCT). Results of this work may also elucidate reasons for the discrepancies in modal mineralogy between previous studies.

The second significant difference between NWA 5790 and the other nakhlites is its apparent lack of “iddingsite” (Corrigan et al. 2013), which comprises finely crystalline secondary minerals including carbonates, Fe-oxides/hydroxides, and clay minerals (e.g., Gooding et al. 1991; Treiman et al. 1993). As veins containing these secondary minerals are cross-cut by fusion crust, they are clearly preterrestrial, and so Martian in origin (Gooding et al. 1991). To be confident that Martian iddingsite does not occur in NWA 5790, we have sought to locate, identify, and determine the origin (i.e., pre- or post-terrestrial) of any minerals that have formed from liquid water. A finding

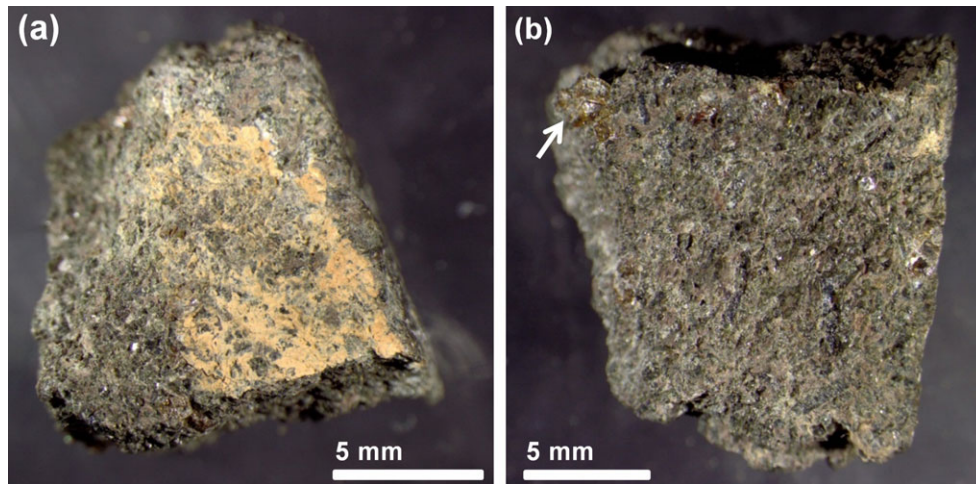


Fig. 1. Images of NWA 5790 chip acquired using a binocular microscope. a) Buff-colored “caliche” coating of one of the outer surfaces. b) The interior of the chip with an olivine grain indicated by an arrow (top left).

that Martian secondary minerals are indeed absent from NWA 5790 would suggest that the part of the igneous body from which it was derived was isolated from the aqueous solutions that interacted with other regions of the flow/sill, and this information may provide fresh constraints on its internal structure and origin.

## MATERIALS AND METHODS

### Initial Sample Characterization

NWA 5790 comprises two stones (total mass 145 g; Weisberg et al. 2010), and this study used a single 2.7 g chip ( $\sim 1.1 \times 1.2 \times 0.8 \text{ cm}^3$ ) from the outer part of one of the stones that was acquired from the Macovich collection. This sample was selected because it provides a profile from the exterior of the meteorite (which is most likely to contain terrestrial weathering products) to the fresh interior. The meteorite’s original outer surface has a fine-grained buff-colored coating that Shih et al. (2010) termed “caliche” (Fig. 1a), whereas the freshly broken interior surfaces of the chip are dark green in color (Fig. 1b). As the interior of the meteorite is free of Fe-(hydr)oxide veins and grain rims, it would be classified as W0 on the thin section weathering scales (Jull et al. 1991; Wlotzka 1993; Al-Kathiri et al. 2005). Given that minerals of a presumed terrestrial origin are visible to the naked eye on the outer sample surface (i.e., the “caliche”), NWA 5790 should have an “E” subclassification.

### X-Ray Computed Tomography

Prior to destructive sampling, the mineralogy and microstructure of the chip were characterized in 3-D

by high-resolution XCT, which is a technique that has previously been used successfully to study Nakhla (Needham et al. 2013). The XCT work employed a Nikon Metris XTH 225 scanner at the University of Manchester (UK) operating with a Cu target at an accelerating voltage of 120 keV. Exactly 3143 projections were collected, with an exposure of 20 s per projection. Reconstruction was performed using Nikon proprietary filtered back projection algorithms, and each reconstructed 3-D image has a resolution of  $10.3 \times 10.3 \times 10.3 \mu\text{m}^3$  per voxel (i.e., 3-D pixel). A 3-D median filter was applied (kernel of  $3 \times 3$ ), and the 3-D image was constructed using Avizo™ software. The bulk mineralogy was determined using grayscale values associated with each voxel to distinguish between regions with contrasting linear attenuation coefficients (i.e., minerals of different density). Modal mineralogy was obtained for the entire data set (which represents only  $\sim 2\%$  of the meteorite by mass but is equivalent in volume to  $\sim 250$  thin sections  $130 \text{ mm}^2$  in size), and for a series of 2-D slices extracted from it. The 2-D slices of the 3-D data set were segmented manually (to minimize the impact of beam hardening and subvoxel variability on segmentation) using the known relative attenuation of the observed mineralogy and the SEM images to define the phases. The 3-D segmentation (Fig. 2) was then performed using the same threshold values. Errors caused by threshold placement and subvoxel variability are difficult to quantify in manually segmented data, but are generally  $<5\%$  for any individual grain  $>125$  voxels when performing global automated analysis. Secondary minerals were not detected with XCT. All quantitative analyses were performed on the 2-D slices, and errors are estimated

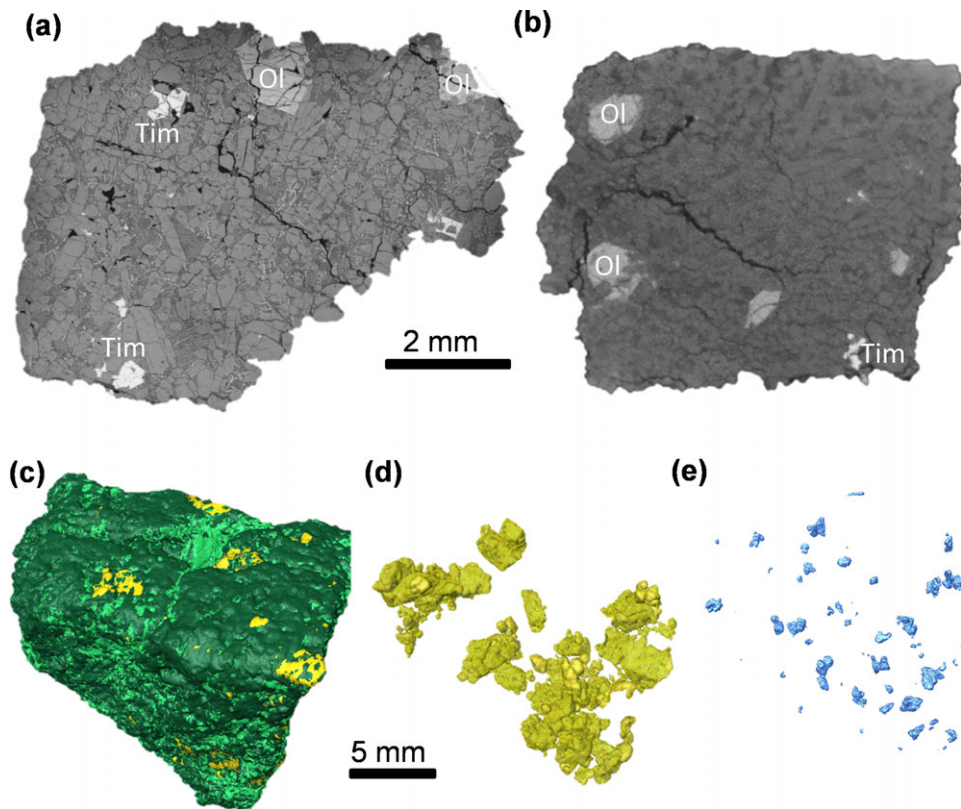


Fig. 2. a) Backscattered electron (BSE) images of the NWA 5790 polished block. It is dominated by augite phenocrysts, between which is the mesostasis (slightly darker gray). The large light gray grains are olivine (Ol), whereas titanomagnetite (Tim) is white and pore space is black. b) An image slice from the XCT data set. Its NWA 5790 XCT slice constituent augite, olivine (Ol), titanomagnetite (Tim), and mesostasis have the same relative grayscale as in the BSE image in (a), but the XCT image has a lower spatial resolution. c) The 3-D rendering of surface of NWA 5790 showing main constituents: dark green denotes augite, light green is mesostasis, and yellow is olivine. d) The 3-D rendering of olivine grains with the other phases transparent; note that the grains are clustered. e) The 3-D rendering of the coarse titanomagnetite grains, again with other components transparent. The voxel resolution of all XCT images is 10.3  $\mu\text{m}$ .

at <0.5%. Mesostasis, augite, olivine, and coarse-grained titanomagnetite were all identified (in order of descending abundance). Owing to high levels of noise in the data from the central portion of the sample, unambiguously distinguishing between augite and the mesostasis in this region was difficult, and so the modal mineralogy of the entire sample could not be obtained with confidence. Instead, interspaced slices were taken and divided into grayscale values for calculation of modal mineralogy. Six were selected to provide a  $\sim 1$  mm interspacing between 2-D slices ( $100 \times 10.3 \mu\text{m}$ ) and therefore increase the chance of sampling discrete grains of olivine and pyroxene (1–2 mm in length). The augite, olivine, and titanomagnetite observed by XCT and SEM (described below) are referred to as “grains” unless information is available to show that they are individual crystals. Unless otherwise stated, crystal/grain sizes quoted are the longest dimension.

### Electron Microscopy

Further information on the proportions, elemental compositions, and petrographic context of individual minerals was obtained by studying a polished block and mineral grains that had been handpicked from the bulk sample using instrumentation at the University of Glasgow. The polished block was made by cutting a slice  $7 \times 6 \text{ mm}^2$  in size from the edge of the bulk sample using an unlubricated saw; this slice was resin impregnated and polished, using glycol as a lubricant in an attempt to preserve any water-soluble minerals. Backscattered electron (BSE) images were obtained from the block using a Zeiss Sigma field-emission SEM operated at 20 kV/1 nA and in low vacuum mode ( $\sim 50$  Pa). Comparison of 2-D XCT images with BSE images shows that contrast differences between minerals are comparable, although the XCT technique has a lower spatial resolution (i.e., 10.3  $\mu\text{m}$  for XCT

versus tens of nanometers for the low vacuum BSE images; Figs. 2a and 2b). The polished block was point counted by traversing over its surface in regular steps and recording the component in the center of the microscope's field of view at each one. The microstructure and crystallographic orientation of calcite and olivine were studied by electron backscatter diffraction (EBSD) using an EDAX-TSL system attached to a FEI Quanta field-emission SEM operated at 20 kV. Prior to EBSD work, the polished block was briefly repolished in colloidal silica. X-ray spectra and maps were acquired from the block after carbon coating and with the Zeiss SEM operated at 20 kV/3 nA. Data were collected using an Oxford Instruments X-Max silicon-drift energy-dispersive X-ray detector operated through Oxford Instruments Aztec software.

Individual olivine crystals and larger polymineralic grains that had been handpicked from the bulk sample were mounted on adhesive carbon tabs for secondary electron (SE) and BSE imaging. Some of these grains were subsequently encapsulated in resin and polished so that their surfaces and near-surface regions could be imaged in cross section. One of the handpicked olivine grains that had a clay mineral covering was gold coated, then electron-transparent foils were cut from its outer surface using a FEI Duomill dual-beam focused ion beam (FIB) instrument operated with a 30 kV Ga<sup>+</sup> ion beam and following the procedure of Lee et al. (2003). The foils were studied initially by low-voltage scanning transmission electron microscopy (LV-STEM) using a STEM detector on the Zeiss SEM that enables acquisition of bright-field and annular dark-field images (Lee and Smith 2006). X-ray spectra were also obtained from the foils to help in mineral identification; these spectra contain AlK<sub>α</sub> and CuK<sub>α</sub> peaks (from the STEM detector and support grid, respectively), which have been removed from the spectra for clarity. Bright-field diffraction contrast images and selected area electron diffraction (SAED) patterns were acquired from the foils using a FEI T20 transmission electron microscope (TEM) operated at 200 kV. The SAED work used a selected area aperture 200 nm in diameter, and the errors on d-spacing determinations are ~0.5–1.0% of the value.

### Chemical and Isotopic Analysis

Chemical and isotopic analysis was used to determine the compositions of NWA 5790 mineral grains, the carbon and oxygen isotope composition of the “caliche” coating, and the hydrogen isotope composition of a clay mineral selvage on olivine. The

chemical compositions of augite and olivine grains in the carbon-coated polished block were obtained by electron probe microanalysis (EPMA). This work used a Cameca SX100 at the University of Edinburgh (UK), which was operated at 15 kV. Calibration used a set of standards established by the Edinburgh EPMA facility: jadeite (Na), spinel (Mg, Al), wollastonite (Si, Ca), orthoclase (K), rutile (Ti), Cr metal (Cr), Mn metal (Mn), fayalite (Fe), and Ni metal (Ni). The beam was set at ~1 μm diameter for all analyses, and two conditions were used: 10 nA for Na, Mg, Si, and Fe, and 100 nA for Al, K, Ca, Ti, Cr, Mn, and Ni. Peak/background counting times were 20/10 s to 40/20 s depending on the element being analyzed. Typical detection limits, in wt%, are as follows: Na<sub>2</sub>O (0.04), MgO (0.03), Al<sub>2</sub>O<sub>3</sub> (0.04), SiO<sub>2</sub> (0.12), K<sub>2</sub>O (0.01), CaO (0.05), TiO<sub>2</sub> (0.01), Cr<sub>2</sub>O<sub>3</sub> (0.02), MnO (0.08), FeO (0.13), and NiO (0.02).

Pieces of the “caliche” coating were handpicked from the chip and analyzed for carbon and oxygen isotopes by reaction with anhydrous H<sub>3</sub>PO<sub>4</sub> at 70 ± 0.1 °C for 24 h to produce CO<sub>2</sub>. An AP2003 continuous-flow mass spectrometer was used to obtain δ<sup>18</sup>O<sub>VSMOW</sub> and δ<sup>13</sup>C<sub>VPDB</sub>, with a reproducibility error of ±0.2‰ (2σ) and ±0.4‰ (2σ), respectively. Three NWA 5790 samples were run interspaced with international standards NBS18, NBS19, and internal laboratory standards for calibration and corrections. A NanoSIMS 50L at the Open University was used to measure the deuterium/hydrogen (D/H) ratio of a clay mineral selvage on an olivine grain surface. Prior to analysis, the olivine grain was pressed into indium. A Cs<sup>+</sup> primary ion beam with a probe current of between 6.0 and 3.7 nA, and a mass resolving power of ~4000 was used for the measurements. Five electron multipliers enabled simultaneous detection of <sup>1</sup>H<sup>-</sup>, <sup>2</sup>H<sup>-</sup>, <sup>12</sup>C<sup>-</sup>, <sup>13</sup>C<sup>-</sup>, <sup>18</sup>O<sup>-</sup>, with the last three isotopes serving as checks for contamination and uniform sputtering. An initial 12 × 12 μm<sup>2</sup> presputter was conducted for 30 s (to remove contamination) before rastering over a 10 × 10 μm<sup>2</sup> area, with data acquired from the inner 5 × 5 μm<sup>2</sup> (25% blanking). Including the presputter, each analysis took 11 min and consisted of 25 blocks of 25 measurements with a count time of 0.14 s per frame. An electron gun was used for charge compensation. A D/H depth profile was obtained by sequentially analyzing and sputtering the same location on the grain surface. The standard used for correcting instrumental mass fractionation was montmorillonite, which has a true δD value of -67‰ (Hallis et al. 2012). Measurements of the montmorillonite were conducted with an elemental analyzer attached to a Thermo MAT 253 gas bench

mass spectrometer. The corrections applied to the montmorillonite data were:

$$\beta_{\text{INS}} = \frac{(^2\text{H}/^1\text{H})_{\text{SIMS}}}{(^2\text{H}/^1\text{H})_{\text{TRUE}}} \quad (1)$$

where  $\beta_{\text{INS}}$  refers to the instrumental mass fractionation of the montmorillonite,  $^2\text{H}/^1\text{H}_{\text{SIMS}}$  is the NanoSIMS value (montmorillonite used for  $\beta_{\text{INS}}$ ), and  $^2\text{H}/^1\text{H}_{\text{TRUE}}$  is the value calculated from the gas bench result. Each measurement on NWA 5790 clay mineral selvage was calculated using:

$$\delta D_{\text{sample}} = \left[ \left( \frac{(^2\text{H}/^1\text{H})_{\text{SIMS}}/\beta_{\text{INS}}}{(^2\text{H}/^1\text{H})_{\text{VSMOW}}} - 1 \right) \right] \times 1000 \quad (2)$$

where  $^2\text{H}/^1\text{H}_{\text{VSMOW}}$  refers to the  $1.557 \times 10^{-6}$  ratio of Vienna Standard Mean Ocean Water. Errors for  $(^2\text{H}/^1\text{H})_{\text{SIMS}}$  and  $\beta_{\text{INS}}$  were calculated according to the standard deviation of the sum of the measured ratios. These errors were calculated as follows:

$$\delta D_{\text{sample error}(2\sigma)} = \left[ \sqrt{(\text{SEEM}^2 + \text{SESM}^2)} \right] \times 2 \quad (3)$$

where SEEM is standard error on each measurement, and SESM is standard error across montmorillonite analyses. Values are quoted in the per mil notation.

## RESULTS

### Modal Mineralogy

The entire 2.7 g chip was scanned by XCT (Fig. 2). Previous work on NWA 5790 and our own observations show that it is dominated by hundreds of micrometer to a few millimeter size grains of augite, olivine, and titanomagnetite, between which is the mesostasis (Figs. 2a and 2b). XCT and BSE images reveal that fractures cross-cut the whole sample and dissect individual grains (Figs. 2a and 2b). The grains of augite, olivine, titanomagnetite, and the volumes of mesostasis could be readily distinguished in the XCT data by differences in their linear attenuation coefficients, but the constituent mineral grains of the mesostasis were too small to individually resolve (Figs. 2a and 2c–e). Table 1 lists mineral abundances derived from individual 2-D XCT slices, and reveals some variation in modal mineralogy between them; mesostasis ranges from 34.7 to 44.2 vol%. and olivine from 2.0 to 5.6 vol%. By appropriately segmenting the XCT data set, the distributions of different minerals throughout the scanned volume can be assessed, and

results show that olivine grains are clustered (Fig. 2d). The polished block was point counted three times (it was rotated in the SEM by  $\sim 30^\circ$  between successive counts), and the values for modal mineralogy thus obtained are close to the mean of the XCT slices (Table 1). Previous determinations of modal mineralogy by Jambon et al. (2010), Weisberg et al. (2010), Mikouchi et al. (2012), and Corrigan et al. (2014) are close to the XCT and point count data in mesostasis abundance, but on average lower in pyroxene and higher in olivine (Table 1).

### Primary Minerals

Augite occurs as zoned euhedral to subhedral phenocrysts that are up to 2 mm in length by 0.1–0.5 mm in width (Fig. 3). The augite grain cores show an irregular zonation and their rims are  $\sim 30 \mu\text{m}$  wide (Fig. 3c). The rims are present where the augite is juxtaposed with mesostasis but absent where in contact with olivine. Relative to the cores, the rims are enriched in Al, Ti, and Fe, and depleted in Mg, Ca, and Cr (Figs. 3b and 3c; Table S1). The composition of the pyroxene core is  $\text{En}_{33.1} \pm 1.6 \text{Fs}_{26.6} \pm 1.6 \text{Wo}_{40.3} \pm 0.7$ , and the rim is  $\text{En}_{20.5} \pm 0.4 \text{Fs}_{40.7} \pm 0.9 \text{Wo}_{38.8} \pm 0.6$  (Fig. 4; Table S1); these results are consistent with values quoted by Jambon et al. (2010).  $\text{Al}_2\text{O}_3$  concentrations of the cores of nakhilite pyroxene crystals have been shown by McKay et al. (2006) to correspond well to the positions of their host meteorites in the lava flow/sill as inferred by other criteria, and in NWA 5790, values range from 0.78 to 1.38 wt% (Fig. 4; Table S1).

Olivine occurs as phenocrysts (Fig. 5a), and much finer acicular crystals in the mesostasis. The olivine grains are subhedral to anhedral,  $\sim 1$ –2 mm in size, and are zoned with a 10–20  $\mu\text{m}$  wide Fe-rich rim. Their core has a mean composition of  $\text{Fa}_{67} \pm 0.5$  (Table S2), which is again consistent with Jambon et al. (2010), who also recorded a composition of  $\text{Fa}_{80}$  from the grain rims. The olivine grains frequently have inclusions 100–250  $\mu\text{m}$  in size of unzoned augite as well as rare melt inclusions comprising grains of augite and titanomagnetite in a feldspathic groundmass (Fig. 5a and 5b); Jambon et al. (2010) and McCubbin et al. (2013) noted that these inclusions can also contain amphibole. The olivine grains contain lamellae of magnetite and augite up to  $\sim 30 \mu\text{m}$  in length by  $\sim 0.7 \mu\text{m}$  in width, which are reminiscent of lamellar symplectites described in other nakhilites (e.g., Mikouchi et al. 2000; Noguchi et al. 2009; Lee et al. 2013). Coarse titanomagnetite grains are 0.2–1 mm in size (Fig. 5c) and contain ilmenite exsolution lamellae.

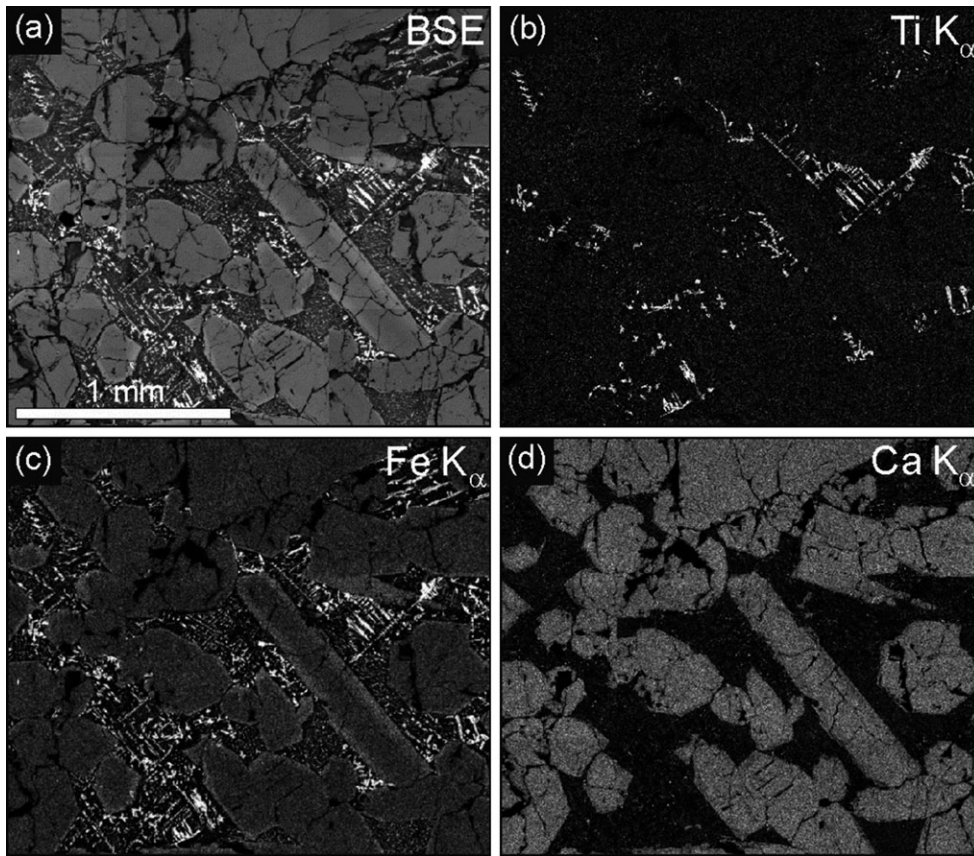


Fig. 3. (a) BSE image and (b–d) X-ray element maps from an area of the NWA 5790 polished block that contains grains of augite (the Ca-rich grains that are light gray in [d]) with mesostasis between them. The augite grains have narrow Fe- and Ti-enriched rims, and the mesostasis contains abundant titanomagnetite dendrites (the white needle-shaped crystals in [b] and [c]). Coarse olivine and titanomagnetite grains are absent from this part of the polished block.

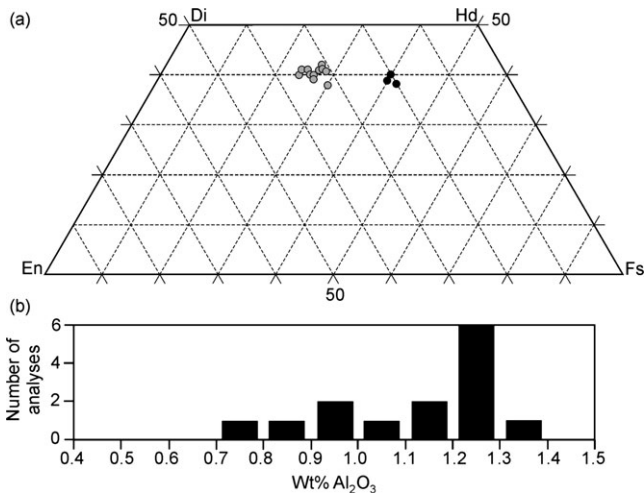


Fig. 4. a) Plot of the composition of NWA 5790 pyroxene grains. The gray symbols are grain cores and black symbols are the rims. b) Histogram showing the range of Al<sub>2</sub>O<sub>3</sub> concentrations in the cores of the pyroxene grains. All of the analyses are listed in Table S1.

The mesostasis of NWA 5790 (Fig. 5d) has been reported to contain plagioclase feldspar (An<sub>16</sub>Ab<sub>79</sub>Or<sub>5</sub>, Jambon et al. 2010; An<sub>20</sub>Ab<sub>71</sub>Or<sub>9</sub>, Mikouchi et al. 2012) together with apatite, silica, Fe-rich olivine, and a Fe-rich glass that may host maskelynite (McCubbin et al. 2013). BSE imaging coupled with qualitative EDX has shown that the Fe-rich olivine occurs as abundant acicular crystals, and the titanomagnetite forms dendritic and cruciform grains, again with ilmenite exsolution lamellae; ~20 μm size grains of alkali feldspar and ~1 μm size grains of Fe-sulfide are also present.

#### “Caliche” Coating

The “caliche” is present on one outer surface of the sample (Figs. 1a and 6a–c), where it forms a buff-colored coating up to ~500 μm thick, but can also extend a few hundred micrometers into the interior of the meteorite along fractures. The coating consists of a loose aggregate of ~1–15 μm size silicate grains,

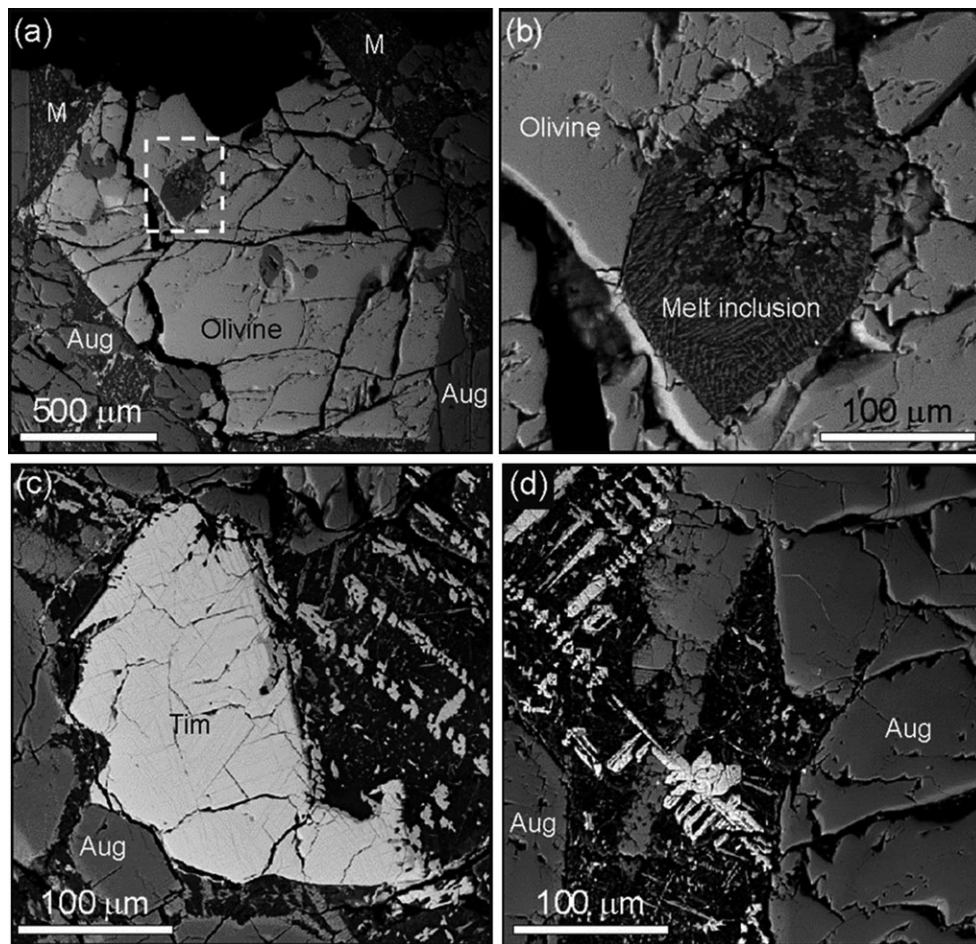


Fig. 5. BSE images of the polished block. a) A fractured olivine phenocryst surrounded by augite (Aug) and mesostasis (M). b) The area within the rectangle in (a) showing a melt inclusion within olivine that contains abundant crystals of Fa-rich olivine. c) A coarse grain of titanomagnetite (Tim) surrounded by augite (Aug) and the mesostasis. d) An area of mesostasis that contains titanomagnetite dendrites (white) between which are augite grains (Aug).

many of which are lozenge shaped (Figs. 6a–c). The mineralogy of most of these grains could not be determined owing to their small size, but qualitative X-ray microanalysis shows that they typically contain O, Al, Si, Mg, Ca, and Fe, and this composition is suggestive of clay minerals. Diatom frustules (silica skeletons of algae) and occasional grains of quartz and biotite also occur. Images of the coating from above reveal that it contains sinuous hollow tubes that are a few micrometers in width by up to 1 mm in length and are encrusted by grains from the coating (Figs. 6a and 6b). The size and shape of these tubes is consistent with the filamentous tubes produced by fungi that are called hyphae. Images of the coating in the polished block show that it contains numerous circular holes that are ~6–10  $\mu\text{m}$  in width, which are likely to be molds of the fungal hyphae in cross section (Fig. 6c). Some parts of the coating have an intergranular calcite cement, and this carbonate extends from the coating into the interior

of the meteorite along veins that cross-cut augite, olivine, and the mesostasis (Figs. 7a and 7b). These calcite veins are up to 60  $\mu\text{m}$  in width by 1 mm in length, and EBSD mapping shows that their constituent calcite is finely polycrystalline. Calcite in the coating has an isotopic composition of  $\delta^{18}\text{O}_{\text{VSMOW}} +26.08 \pm 0.2\%$  ( $2\sigma$ ),  $\delta^{13}\text{C}_{\text{VPDB}} -0.25 \pm 0.4\%$  ( $2\sigma$ ). The C and O isotopic compositions of carbonates in other nakhlite meteorites (from Grady et al. 2007) are compared with the data from NWA 5790 in Fig. 7c.

### Clay Minerals

The outer surfaces of some of the olivine grains immediately beneath the “caliche” have <1–5  $\mu\text{m}$ -sized faceted depressions (Fig. 8a) that are similar in size and shape to etch pits in Nakhla olivine grains (Lee et al. 2013). These grain surfaces may also be covered by one or more very thin layers of a silicate (Fig. 8b), and when

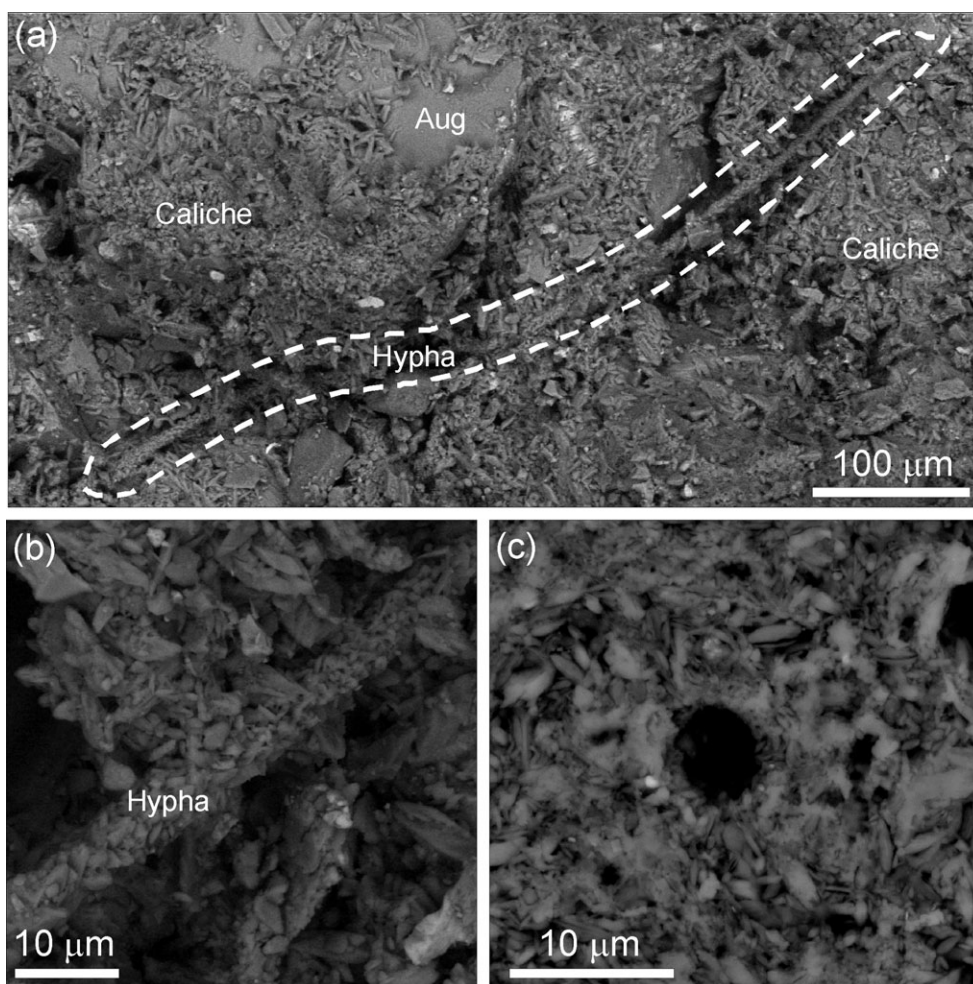


Fig. 6. BSE images of the outer surface of the chip with its “caliche” coating. a) Caliche on a grain of augite (Aug). The caliche is composed of small grains of “dust,” and contains a sinuous tube (highlighted by the dashed white line), whose size and shape is consistent with it being a fungal hypha (labeled). b) Part of the fungal hypha that is encrusted with mineral grains. c) The caliche coating as seen in the polished block. It is an aggregate of mineral grains, but contains many small circular holes (black) that are interpreted to be molds of fungal hyphae.

viewed in cross section, the layers are submicrometer in thickness (Figs. 8c and 9a). TEM images of foils cut from the selvage using the FIB technique reveal that it contains two layers with an irregular contact between them (Fig. 9b). SAED shows that both layers are very finely crystalline, and the two most prominent rings in their patterns have d-spacings of 0.252 and 0.145 nm (Fig. 9c). X-ray spectra obtained by LV-STEM demonstrate that the selvage is a Fe-silicate that is depleted in Mg relative to the underlying olivine (Figs. 9d–f). The inner layer differs from the outer one in having a lower Fe/Si ratio and higher Mg/Si and Ca/Si ratio (Figs. 9e and 9f). These results suggest that the selvage is composed of one or more finely crystalline clay minerals, and a hydrous composition is supported by results from the NanoSIMS depth profile, which show

that  $H^+$  counts are relatively high in its outermost parts (i.e., within the selvage) and decrease toward the olivine substrate (Fig. 10).  $\delta D$  values range from  $-212 \pm 109\%$  ( $2\sigma$ ) to  $-96 \pm 132\%$  ( $2\sigma$ ), with the lowest values coming from the clay minerals and highest values from olivine beneath the selvage (Fig. 10).

Clay minerals are also present as narrow ( $\sim 1 \mu m$  wide) veins within olivine grains. The volumetric abundance of these clay mineral veins can be estimated by assuming that each olivine grain contains a single vein 1.5 mm in length by 1  $\mu m$  in width, although this is likely to be a substantial overestimate. Thus, an olivine grain  $1.5 \times 1.5 \text{ mm}^2$  in size will contain 0.07% clay, and assuming that olivine comprises 4.0 vol% of the meteorite (the mean of data in Table 1), then the abundance of clay minerals in NWA 5790 is 0.003 vol%.

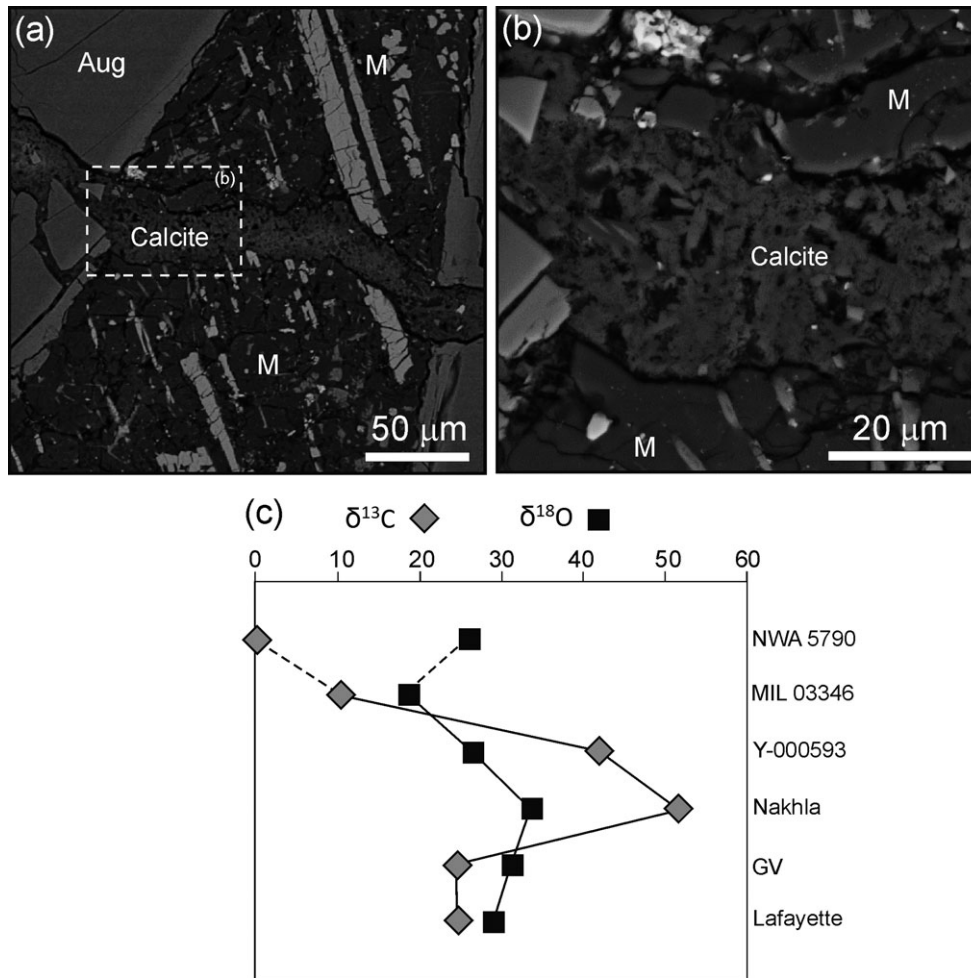


Fig. 7. a) BSE image of the polished block showing a vein of calcite cross-cutting augite (Aug) and the mesostasis (M). b) BSE image of the boxed area in (a) highlighting the relationship between the porous vein of calcite and the mesostasis (M). c) The carbon and oxygen isotopic compositions of carbonate minerals in nakhlite meteorites plotted against their inferred depth within the lava flow/sill. Data are from Grady et al. (2007), with the NWA 5790 values from the present study. Relative depths are after Harvey and McSween (1992) and Mikouchi et al. (2006, 2012). GV denotes Governador Valadares.

## DISCUSSION

### Modal Mineralogy of NWA 5790 and its Position within the Nakhlite Lava Flow/Sill

XCT data and SEM images acquired for the present study confirm that mesostasis is abundant in the piece of NWA 5790 that we have studied. The mean volume of mesostasis, which was calculated by combining results from the present study with previous work ( $38.1 \pm 3.6$  vol%), is considerably greater than the next most mesostasis-rich nakhlite described to date (i.e., 26.4 vol% in MIL 090136; Udry and McSween 2012) (Fig. 11). Such a result is therefore consistent with NWA 5790 having been derived from close to one of the rapidly cooled margins of the nakhlite lava flow/sill. This interpretation is supported by the  $\text{Al}_2\text{O}_3$

concentrations of pyroxene cores (Corrigan et al. 2014). McKay et al. (2006) showed that mean  $\text{Al}_2\text{O}_3$  values are greatest in those meteorites that are inferred to have been derived from the most rapidly cooled part of the igneous body, and the mean value for NWA 5790 of 1.1 wt% (Fig. 4b) is substantially greater than for all of the other nakhlites.

The XCT data show that NWA 5790 is heterogeneous in mineralogy at the subcentimeter scale, and this feature of the rock is highlighted by XCT images showing clustering of olivine (Fig. 2d). The heterogeneous distributions of minerals and mesostasis is also demonstrated by the ~10 vol% range in abundance of pyroxene and mesostasis between individual measurements, and the 7.1 vol% variation in olivine abundance (Table 1; Fig. 11). However, multiple measurements of other nakhlites give similar or greater

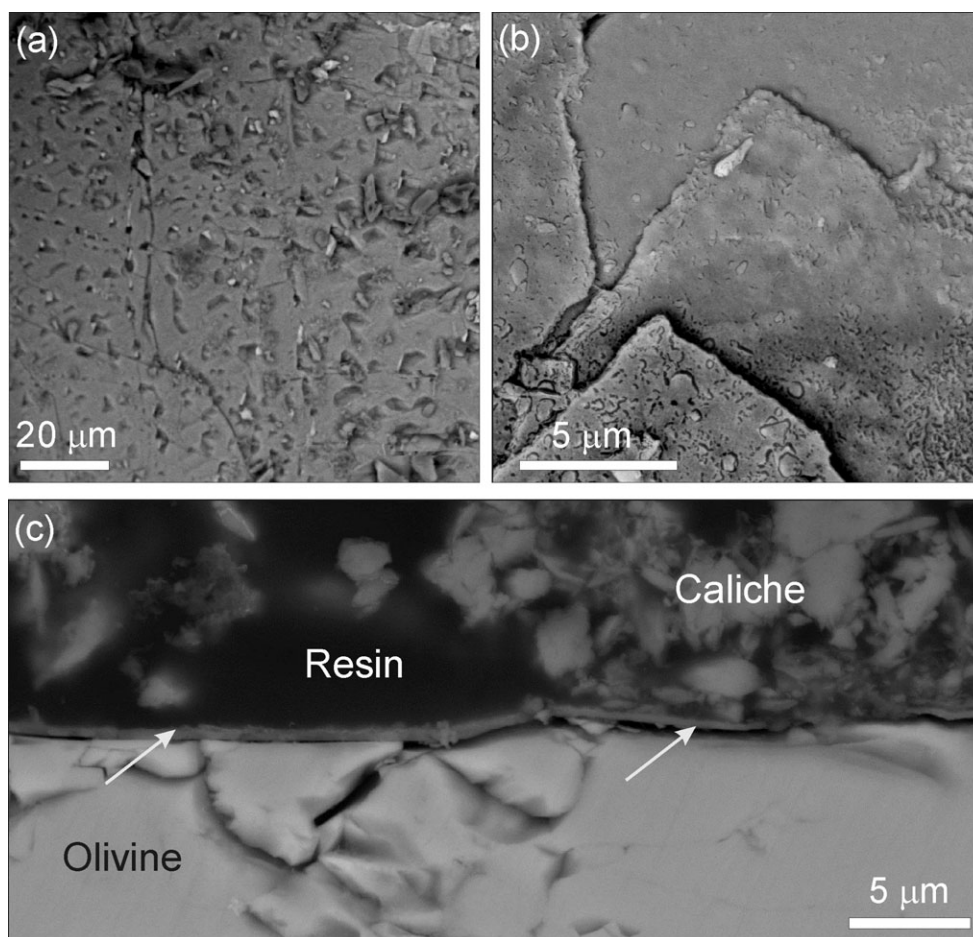


Fig. 8. BSE images of olivine grains exposed at the outer surface of the meteorite, and immediately beneath the caliche. a) The surface of an olivine grain with many small depressions that are reminiscent of etch pits described from Nakhla olivine grains by Lee et al. (2013). b) Thin clay mineral layers on an olivine grain surface. c) A selvage of clay minerals (arrowed) on the surface of an olivine grain that had been handpicked from the outer surface of the meteorite chip, mounted in resin, and polished.

ranges, as illustrated in Fig. 11. The greatest variation is between 27 measurements of Nakhla (ranges of 21.7 vol% pyroxene, 11.0 vol% mesostasis, 26.1 vol% olivine; Needham et al. 2013), whereas four measurements of Lafayette have a narrower spread (ranges of 14.7 vol% pyroxene, 2.4 vol% mesostasis, 12.6 vol% olivine; Friedman-Lentz et al. 1999). The range of Lafayette data is similar to that of four measurements from the paired MIL finds (range of 14.1 vol% pyroxene, 6.6 vol% mesostasis, 8.7 vol% olivine; Day et al. 2006; Udry and McSween 2012). Three measurements of Governador Valadares show a similar range to NWA 5790 (9.6 vol% pyroxene, 4.0 vol% mesostasis, 6.2 vol% olivine; Friedman-Lentz et al. 1999). The contrasts between nakhlites in their heterogeneity are perhaps related to the sizes of the samples studied rather than intrinsic differences in the nature of the rock, but nonetheless, the data listed

above and comparisons in Fig. 11 show that NWA 5790 is relatively uniform in its mineralogy.

#### Origin of the “Caliche” Coating

Shih et al. (2010) suggested that the carbonate-rich coating on NWA 5790 is a “desert contaminant.” This conclusion is consistent with findings of the present study showing that it occurs on only one side of the sample, which is presumably an original outer surface of the meteorite. The coating is a very fine-grained aggregate of silicate mineral grains, which suggests that it originated as wind-blown dust rather than being a true caliche (i.e., a calcareous soil), although the coating does have a patchy calcite cement (discussed below). The intimate association of fungi with the coating indicates that their hyphae have helped to bind the silicate dust. Fungal hyphae have also been found on

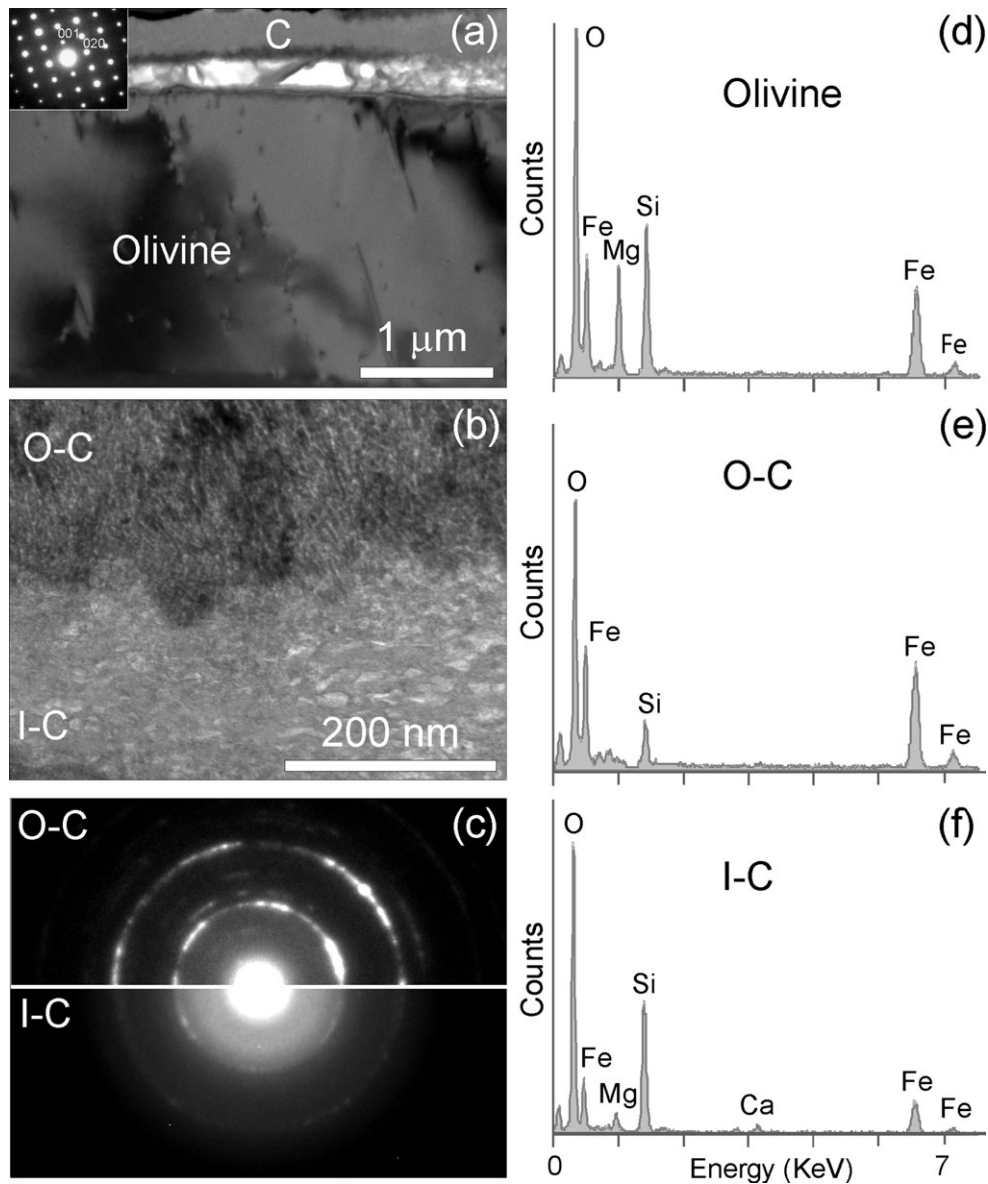


Fig. 9. a) Bright-field TEM image of a foil that was cut normal to the outer surface of the olivine grain in Fig. 8b. The image shows the clay selvage (C) and underlying olivine; the selvage has partly detached from the olivine grain surface. The inset [100] SAED pattern of the olivine shows that it contains linear defects oriented parallel to the trace of (020). b) Bright-field image of the clay mineral selvage showing that it has an inner layer (I-C, which is in contact with the olivine) and an outer layer (O-C). c) SAED patterns of the outer and inner layers of the clay mineral selvage. The two most prominent rings in both patterns have d-spacings of 0.252 and 0.145 nm. d–f) X-ray spectra of the olivine, the outer layer of the clay mineral selvage (O-C), and the inner layer (I-C). They show that microstructural differences between these layers correspond to chemical contrasts. These three spectra contained Al and Cu peaks from the STEM detector and grid holder, respectively, which have been removed for clarity.

the outer surface of Tatahouine, which is a diogenite that fell in Tunisia in 1931 (Benzerara et al. 2005). Toporski and Steele (2007) used Nakhla for experiments to assess its susceptibility to microbial colonization, but identified fungi on a specimen that had been recovered in 1913 even at the start of the experiments. The microbial colonization of NWA 5790 further highlights

the susceptibility of meteorite finds to terrestrial biological contamination.

#### Evidence for Water–Rock Interaction

NWA 5790 contains calcite and clay minerals, both of which occur on the outer surface of the sample and

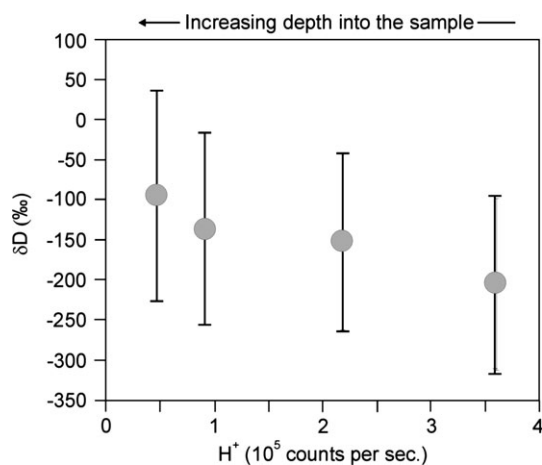


Fig. 10. Hydrogen isotope depth profile through the clay selvage on an olivine grain. The results are expressed as  $\delta D$  versus  $H^+$  counts. The individual  $\delta D$  values with  $2\sigma$  errors are  $-212 \pm 109\text{‰}$ ,  $-157 \pm 111\text{‰}$ ,  $-140 \pm 122\text{‰}$ , and  $-96 \pm 132\text{‰}$ .

extend into the interior of the meteorite as veins. Veins containing carbonates and hydrous silicates, often accompanied by Fe-hydroxides and sulfates, are commonplace in the nakhlites including Nakhla (Gooding et al. 1991; Lee et al. 2013), Lafayette (Treiman et al. 1993; Changela and Bridges 2011; Tomkinson et al. 2013), the paired Miller Range finds (Harris and Taylor 2011), and Y-000593 (Noguchi et al. 2009). As these veins in other nakhlites are cross-cut by fusion crust (Gooding et al. 1991; Treiman et al. 1993), their constituent minerals are clearly preterrestrial (i.e., formed by water–rock interaction on Mars). Below, we explore whether the calcite and clay minerals in NWA 5790 are also Martian, or are products of terrestrial weathering.

### Origin of the Calcite Veins

Several lines of evidence indicate that the calcite veins in NWA 5790 are products of terrestrial weathering rather than having formed on Mars. (1) Martian carbonates in the nakhlites are typically rich in Mn and Fe (e.g., Ca-siderite; Vicenzi et al. 1997), whereas the carbonate in NWA 5790 is nearly pure calcite; (2) veins formed by Martian aqueous alteration are most abundant within nakhlite olivine grains (e.g., Lee et al. 2013; Tomkinson et al. 2013), whereas those in NWA 5790 cross-cut augite, olivine, and the mesostasis; (3) some of the NWA 5790 veins are continuous with the “caliche” coating, which as discussed above is terrestrial in origin; and (4) demonstrably terrestrial calcite veins have been described from other Martian meteorites recovered from hot deserts, including the shergottite Dar al Gani 476

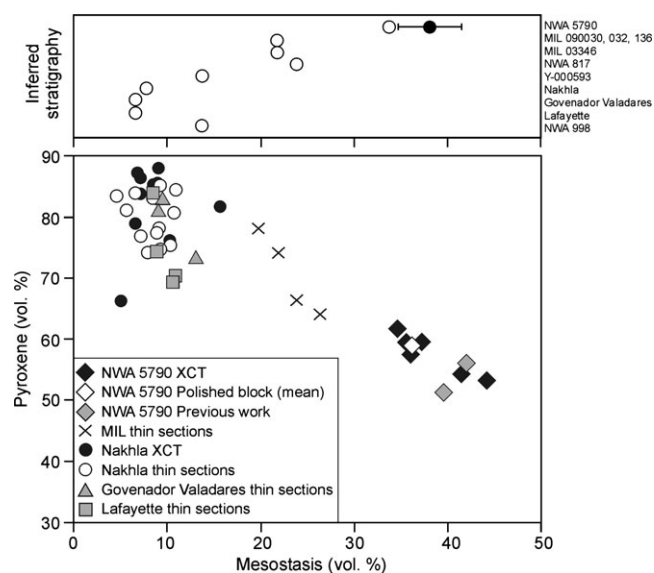


Fig. 11. The lower graph is a plot of the abundance of pyroxene and mesostasis in NWA 5790 compared with data from other nakhlites (values for NWA 5790 are listed in Table 1). MIL data were obtained from thin sections of the paired meteorites MIL 03346, 090030, 090032, and 090136 (Day et al. 2006; Udry and McSween 2012). The Nakhla XCT values are from Needham et al. (2013), and the Nakhla thin section abundances are from Friedman-Lentz et al. (1999) and Needham et al. (2013). Data for the Governor Valadares and Lafayette thin sections are from Friedman-Lentz et al. (1999). The upper graph shows the abundance of mesostasis in all of the nakhlites plotted against their inferred depth of burial. The open symbols are data from Mikouchi et al. (2012), whereas the filled symbol is the overall mean for NWA 5790 (Table 1).

(Coulson et al. 2007) and the nakhlite NWA 998 (Grady et al. 2007; Treiman and Irving 2008).

Given the terrestrial origin for NWA 5790 calcite, it is instructive to compare its carbon and oxygen isotope compositions to those of carbonates from other nakhlites. Grady et al. (2007) compiled  $\delta^{13}\text{C}$  and  $\delta^{18}\text{O}$  values for carbonates in Governor Valadares, Lafayette, MIL 03346, Nakhla, and Y-000593. They highlighted an apparent fall in  $\delta^{13}\text{C}$  close to the chilled margin of the nakhlite lava flow/sill (Fig. 7c). Of the meteorites studied by Grady et al. (2007), MIL 00346 is the nearest to the margin and isotopically lightest. NWA 5790 is likely to have originated from even closer to the margin of the flow/sill than MIL 03346, and its carbonates have commensurately lighter  $\delta^{13}\text{C}$  values (Fig. 7c). Although it is tempting to interpret the carbon isotope composition of NWA 5790 calcite in terms of the model of Grady et al. (2007), its  $\delta^{13}\text{C}$  value of  $-0.25 \pm 0.4\text{‰}$  reflects a terrestrial origin, and so suggests that there may also be a terrestrial contribution to carbonates in the Antarctic finds MIL 03346 and Y-000593. The  $\delta^{18}\text{O}$  value of NWA 5790 calcite is

similar to that of the other nakhlites, but as it formed on Earth, these data show that  $\delta^{18}\text{O}$  alone cannot be used to distinguish Martian from terrestrial carbonates.

### Origin of the Clay Minerals

The abundance of clay minerals in NWA 5790 (i.e.,  $\sim 0.003$  vol%) is far lower than in the other seven nakhlites, which contain olivine-hosted secondary mineral veins that are sufficiently large and abundant to be readily identifiable by light microscopy and BSE imaging (e.g., Ashworth and Hutchison 1975; Bunch and Reid 1975; Berkley et al. 1980; Treiman et al. 1993; Gillet et al. 2002; Imae et al. 2003; Day et al. 2006; Treiman and Irving 2008). Estimated abundances of secondary minerals include 0.24 vol% for MIL 03346 (Day et al. 2006) and  $\sim 1$  wt% for Nakhla (Gooding et al. 1991; Leshin et al. 1996). However, despite their lower abundance, the NWA 5790 clay minerals are similar in petrographic context to those described from the other nakhlites (i.e., occurring as narrow olivine-hosted veins), and so could be Martian in origin. The selvages of clay minerals that line the surfaces of olivine grains immediately beneath the “caliche” may have originally been part of an olivine-hosted vein. These clay minerals would have been exposed as the olivine grain broke apart along the line of the vein during terrestrial weathering; this newly formed grain surface was subsequently coated with silicate dust. Indeed, the propensity of olivine grains to break along secondary mineral veins was utilized by Lee et al. (2013) to study the internal structure of veins of Martian iddingsite in Nakhla. A Martian origin for the NWA 5790 clay minerals is also supported by their compositional and structural similarity to olivine-hosted veins of smectite described from Nakhla (Lee et al. 2013). The Nakhla smectite is Fe-rich, and the most prominent reflections in its SAED patterns have d-spacings of 0.257 nm and 0.157 nm (the NWA 5790 clay minerals have d-spacings of 0.252 and 0.145 nm).

The provenance of NWA 5790 clay minerals can be tested using results from the D/H analyses. Terrestrial  $\delta\text{D}$  ranges from  $-400$  to  $+50\text{‰}$  (Hoefs 2009), whereas the Martian atmosphere has a much higher D/H value owing to the preferential loss of H to space through Jeans escape (Owen et al. 1988). Values for Mars that have been obtained by analysis of hydrous and nominally anhydrous minerals in Martian meteorites, and fall between  $-269$  and  $+5079\text{‰}$  (Watson et al. 1994; Leshin et al. 1996; Saxton et al. 2000; Gillet et al. 2002; Boctor et al. 2003; Vicenzi et al. 2007; Hallis et al. 2012; Usui et al. 2012). However, the lower part of the Martian range is at least partially due to terrestrial contamination; for example, Hallis et al.

(2012) found that clay minerals in Nakhla, which fell in 1911, have undergone substantial isotopic equilibration with the terrestrial environment so that their  $\delta\text{D}$  values range from  $-117 \pm 85\text{‰}$  to  $+1165 \pm 116\text{‰}$ . Therefore, while a  $\delta\text{D}$  in excess of  $+50\text{‰}$  would indicate a Martian origin for the NWA 5790 clay minerals, values lower than this could be consistent with either a Martian or terrestrial provenance. To determine the D/H ratio of the NWA 5790 clay mineral selvage, a depth profile was obtained, which extended from the clay into the olivine beneath, and over this distance  $\delta\text{D}$  increases from  $-212 \pm 109\text{‰}$  to  $-96 \pm 132\text{‰}$  (Fig. 10). As  $\text{H}^+$  counts decrease through the depth profile, it is reasonable to assume that the outermost analyses were from the clay minerals, whereas the innermost ones will have contained a contribution from the olivine substrate.

The  $\delta\text{D}$  values of NWA 5790 clay minerals lie within the range of terrestrial water and previous D/H analyses of minerals within Martian meteorites including veins of Martian iddingsite. Thus, the  $\delta\text{D}$  values of the clay minerals suggest that they could have formed by weathering on Earth, or they may have precipitated in equilibrium with the D-enriched Martian atmosphere and subsequently undergone isotopic exchange with the terrestrial environment. A similar problem was discussed by Gillet et al. (2002), who used D/H analysis in an attempt to determine the origin of Fe-rich smectite in NWA 817, which is another hot desert nakhlite find. A Martian origin for the NWA 817 clays was suggested by their occurrence within serrated veins, which is a very similar petrographic context to indisputably Martian clay minerals and phyllosilicates in Lafayette and Nakhla (e.g., Treiman et al. 1993; Changela and Bridges 2011; Lee et al. 2013; Tomkinson et al. 2013). The mean  $\delta\text{D}$  for NWA 817 smectite was  $-170 \pm 14\text{‰}$ , and although this value is not definitively Martian, Gillet et al. (2002) attributed the low  $\delta\text{D}$  values to precipitation in equilibrium with a Martian reservoir that was out of isotopic equilibrium with the planet's atmosphere (i.e., the mantle). However, both Boctor et al. (2003) and Hallis et al. (2012) have suggested that  $\delta\text{D}$  results from the NWA 817 smectite could also be explained by terrestrial contamination.

Results from the petrographic, chemical, and isotopic analysis of clay minerals in NWA 5790 are therefore inconclusive. A terrestrial origin would, however, be consistent with the occurrence of clay minerals as terrestrial weathering products within ordinary chondrite finds (Bland et al. 2000; Lee et al. 2003; Lee and Bland 2004). Clay minerals are also a major constituent of “desert varnish” that occurs on meteorites that have been recovered from the Sahara and the Nullarbor Plain (Australia) (Lee and Bland

2003). The etch pits on NWA 5790 olivine grains suggest that cations for the clay minerals could have been sourced from their substrate.

A similar question of provenance has been raised with regard to other minerals that form veins in Antarctic nakhlites. The Miller Range meteorites contain gypsum and jarosite veins (McCubbin 2009; Hallis and Taylor 2011; Velbel 2012; Stopar et al. 2013), and jarosite has also been found in the Yamato nakhlites (Treiman and Steele 2008; Noguchi et al. 2009). It remains unclear whether all of the jarosite is a terrestrial weathering product given that jarosite within MIL 03346 has a Martian D/H signature (Vicenzi et al. 2007).

### Implications for Understanding the Internal Structure of the Nakhlite Body

NWA 5790 differs from the other nakhlites with respect to its modal mineralogy and scarcity or absence of Martian secondary minerals. Thus, insufficient volumes of Martian groundwaters penetrated into the margins of the nakhlite lava flow/sill to significantly alter the rock. The paucity of evidence for Martian alteration may simply reflect the distance of NWA 5790 from the source of fluids, but its mineralogy may also have contributed to isolating the rock from groundwaters. Specifically, evidence from Lafayette and Nakhla show that partial dissolution of olivine during early stages of fluid ingress would have substantially increased the porosity and permeability of the lava flow/sill (Lee et al. 2013; Tomkinson et al. 2013). Thus, the paucity of olivine in NWA 5790, and clustering of grains where they do occur, could have served to limit the extent to which new pore space was formed by early dissolution.

## CONCLUSIONS

NWA 5790 provides important new insights into the crystallization history and internal structure of its parent lava flow/sill, and the nature of water-mediated alteration of the Martian crust. Key findings are as follows:

1. NWA 5790 has the greatest abundance of mesostasis among the nakhlites ( $38.1 \pm 3.6$  vol%).
2. Taken together with the zoning of its coarse augite and olivine grains and the high  $\text{Al}_2\text{O}_3$  contents of augite grain cores, the modal mineralogy of NWA 5790 is consistent with crystallization within the chilled margin of a lava flow/sill.
3. One of the outer surfaces of the meteorite has a “caliche” coating that formed by the binding of terrestrial desert dust by a fungal meshwork.

4. The microbial coating was cemented by calcite, and this carbonate has also penetrated into the interior of the meteorite along veins.
5. Very finely crystalline and Fe-rich clay minerals are associated with olivine grains. Neither their petrographic context nor  $\delta\text{D}$  values can be used to distinguish between a Martian or terrestrial origin, but even if they did form on Mars, they are very rare relative to clay minerals and phyllosilicates in the other nakhlites.
6. The scarcity or absence of Martian secondary minerals from NWA 5790 highlights a heterogeneity in access of groundwaters to the parent lava flow/sill of the nakhlites. This may reflect a physical separation of the source area of NWA 5790 from the other nakhlites, or spatial variations in fluid access stemming from contrasts in the volumetric abundance of highly reactive olivine grains.

*Acknowledgments*—We thank Peter Chung (School of Geographical and Earth Sciences, University of Glasgow) for support with the SEM and Billy Smith and Colin How (School of Physics and Astronomy, University of Glasgow) for assistance with FIB and TEM work. For C and O isotope composition work, we thank Terry Donnelly and Julie Dougans. We are grateful to Peter Lee for access to the Manchester X-Ray Imaging Facility, Tristan Lowe for help with XCT data collection, and Chris Hayward (University of Edinburgh) for assistance with the EPMA. The sample was acquired from the Macovitch collection, New York. Grant funding from UK Science and Technology Facilities Council (ST/H002472/1 and ST/H002960/1) is gratefully acknowledged. This manuscript has benefitted considerably from careful reviews by Cari Corrigan and two anonymous referees.

*Editorial Handling*—Dr. Cyrena Goodrich

## REFERENCES

- Agee C. B., Wilson N. V., McCubbin F. M., Ziegler K., Polyak V. J., Sharp Z. D., Asmerom Y., Nunn M. H., Shaheen R., Thiemens M. H., Steele A., Fogel M. L., Bowden R., Glamoclija M., Zhang Z., and Elardo S. M. 2013. Unique meteorite from early Amazonian Mars: Water-rich basaltic breccia Northwest Africa 7034. *Science* 339:780–785.
- Al-Kathiri A., Hofmann B. A., Jull A. J. T., and Gnos E. 2005. Weathering of meteorites from Oman: Correlation of chemical and mineralogical weathering proxies with  $^{14}\text{C}$  terrestrial ages and the influence of soil chemistry. *Meteoritics & Planetary Science* 40:1215–1239.
- Ashworth J. R. and Hutchison R. 1975. Water in non-carbonaceous stony meteorites. *Nature* 256:714–715.
- Basu Sarbadhikari A., Goodrich C. A., Liu Y., Day J. M. D., and Taylor L. A. 2011. Evidence for heterogeneous

- enriched shergottite mantle sources in Mars from olivine-hosted melt inclusions in Larkman Nunatak 06319. *Geochimica et Cosmochimica Acta* 75:6803–6820.
- Benzerara K., Menguy N., Guyot F., Vanni C., and Gillet P. 2005. TEM study of a silicate-carbonate-microbe interface prepared by focused ion beam milling. *Geochimica et Cosmochimica Acta* 69:1413–1422.
- Berkley J. L., Keil K., and Prinz M. 1980. Comparative petrology and origin of Governador Valadares and other nakhlites. Proceedings, 11th Lunar and Planetary Science Conference. pp. 1089–1102.
- Bland P. A., Lee M. R., Sexton A. S., Franchi I. A., Fallick A. E. T., Miller M. F., Cadoga J. M., Berry F. J., and Pillinger C. T. 2000. Aqueous alteration without a pronounced oxygen isotope shift: Implications for asteroidal processing of chondritic materials. *Meteoritics & Planetary Science* 35:1387–1395.
- Boctor N. Z., Alexander C. M. O'D., Wang J., and Hauri E. 2003. The sources of water in Martian meteorites: Clues from hydrogen isotopes. *Geochimica et Cosmochimica Acta* 67:3971–3989.
- Bunch T. E. and Reid A. M. 1975. The nakhlites Part 1: Petrography and mineral chemistry. *Meteoritics* 10:303–315.
- Cartwright J. A., Ott U., Herrmann S., and Agee C. B. 2014. Modern atmospheric signatures in 4.4 Ga Martian meteorite NWA 7034. *Earth & Planetary Science Letters* 400:77–87.
- Changela H. G. and Bridges J. C. 2011. Alteration assemblages in the nakhlites: Variation with depth on Mars. *Meteoritics & Planetary Science* 45:1847–1867.
- Corrigan C. M., Velbel M. A., Vicenzi E. P., and Konicek A. 2013. Nakhlite NWA 5790: Modal mineralogy and comparison with the rest of the nakhlites. *Meteoritics & Planetary Science* 48:A5309.
- Corrigan C. M., Velbel M. A., Vicenzi E. P., and Konicek A. 2014. Modal mineralogy and chemistry of nakhlite Northwest Africa (NWA) 5790: How it stacks up with the rest of the nakhlites (abstract #2128). 45th Lunar and Planetary Science Conference. CD-ROM.
- Coulson I. M., Beech M., and Nie W. 2007. Physical properties of Martian meteorites: Porosity and density measurements. *Meteoritics & Planetary Science* 42:2043–2054.
- Day J. M. D., Taylor L. A., Floss C., and McSween H. Y. 2006. Petrology and chemistry of MIL 03346 and its significance in understanding the petrogenesis of nakhlites on Mars. *Meteoritics & Planetary Science* 41:581–606.
- Friedman-Lentz R. C., Taylor G. J., and Treiman A. H. 1999. Formation of a Martian pyroxenite: A comparative study of the nakhlite meteorites and Theo's Flow. *Meteoritics & Planetary Science* 34:919–932.
- Fritz J., Artemieva N., and Greshake A. 2005. Ejection of Martian meteorites. *Meteoritics & Planetary Science* 40:1393–1411.
- Gillet P., Barrat J.-A., Deloule E., Wadhwa M., Jambon A., Sautter V., Devouard B., Neuville D., Benzerara K., and Lesourd M. 2002. Aqueous alteration in the Northwest Africa 817 (NWA 817) Martian meteorite. *Earth and Planetary Science Letters* 203:431–444.
- Gooding J. L., Wentworth S. J., and Zolensky M. E. 1991. Aqueous alteration of the Nakhla meteorite. *Meteoritics* 26:135–143.
- Grady M. M., Anand M., Gilmour M. A., Watson J. S., and Wright I. P. 2007. Alteration of the Nakhlite Lava Pile: Was water on the surface, seeping down, or at depth, percolating up? Evidence (such as it is) from carbonates (abstract #1826). 38th Lunar and Planetary Science Conference. CD-ROM.
- Hallis L. J. and Taylor G. J. 2011. Comparisons of the four Miller Range nakhlites, MIL 03346, 090030, 090032 and 090136: Textural and compositional observations of primary and secondary mineral assemblages. *Meteoritics & Planetary Science* 46:1787–1803.
- Hallis L. J., Taylor G. J., Nagashima K., Huss G. R., Needham A. W., Grady M. M., and Franchi I. A. 2012. Hydrogen isotope analyses of alteration phases in the nakhlite Martian meteorites. *Geochimica et Cosmochimica Acta* 97:105–119.
- Harvey R. P. and McSween H. Y. 1992. The parent magma of the nakhlites: Clues from melt inclusions. *Earth and Planetary Science Letters* 111:467–482.
- Hoefs J. 2009. *Stable isotope geochemistry*, 6th ed. Berlin: Springer.
- Huber L., Irving A. J., Maden C., and Wieler R. 2012. Noble gas cosmic ray exposure ages of four unusual Martian meteorites: Shergottites NWA 4797, NWA 5990, NWA 6342 and Nakhlite NWA 5790 (abstract #1408). 43rd Lunar and Planetary Science Conference. CD-ROM.
- Humayun M., Nemchin A., Zanda B., Hewins R. H., Grange M., Kennedy A., Lorand J. P., Gopel C., Fieni C., Pont S., and Deldicque D. 2013. Origin and age of the earliest Martian crust from meteorite NWA 7533. *Nature* 503:513–516.
- Imae N., Ikeda Y., Shinoda K., Kojima H., and Iwata N. 2003. Yamato nakhlites: Petrography and mineralogy. *Antarctic Meteorite Research* 16:13–33.
- Jambon A., Barrat J.-A., Bollinger C., Sautter V., Boudouma O., Greenwood R. C., Franchi I. A., and Badia D. 2010. Northwest Africa 5790. Top sequence of the Nakhlite pile (abstract #1696). 41st Lunar and Planetary Science Conference. CD-ROM.
- Jull A. J. T., Wlotzka F., and Donahue D. J. 1991. Terrestrial ages and petrologic description of Roosevelt County meteorites (abstract). 32nd Lunar and Planetary Science Conference. p. 667.
- Korochantseva E. K., Schwenzer S. P., Buikin A. I., Hoppe J., Ott U., and Trieloff M. 2011. <sup>40</sup>Ar–<sup>39</sup>Ar and cosmic-ray exposure ages of nakhlites—Nakhla, Lafayette, Governador Valadares and Chassigny. *Meteoritics & Planetary Science* 46:1397–1417.
- Lee M. R. and Bland P. A. 2003. Dating climatic change in hot deserts using desert varnish on meteorite finds. *Earth and Planetary Science Letters* 206:187–198.
- Lee M. R. and Bland P. A. 2004. Mechanisms of weathering of meteorites recovered from hot and cold deserts and the formation of phyllosilicates. *Geochimica et Cosmochimica Acta* 68:893–916.
- Lee M. R. and Smith C. L. 2006. Scanning transmission electron microscopy using a SEM: Applications to mineralogy and petrology. *Mineralogical Magazine* 70:561–572.
- Lee M. R., Bland P. A., and Graham G. 2003. Preparation of TEM samples by focused ion beam (FIB) techniques: Applications to the study of clays and phyllosilicates in meteorites. *Mineralogical Magazine* 67:581–592.
- Lee M. R., Tomkinson T., Mark D. F., Smith C. L., and Stuart F. M. 2013. Evidence for silicate dissolution on

- Mars from the Nakhla meteorite. *Meteoritics & Planetary Science* 48:224–240.
- Leshin L. A., Epstein S., and Stolper E. M. 1996. Hydrogen isotope geochemistry of SNC meteorites. *Geochimica et Cosmochimica Acta* 60:2635–2650.
- McCubbin F. M. 2009. Hydrothermal jarosite and hematite in a pyroxene-hosted melt inclusion in Martian meteorite Miller Range (MIL) 03346: Implications for magmatic-hydrothermal fluids on Mars. *Geochimica et Cosmochimica Acta* 73:4907–4917.
- McCubbin F. M., Elardo S. M., Shearer C. K. Jr., Smirnov A., Hauri E. H., and Draper D. S. 2013. A petrogenetic model for the co-magmatic origin of chassignites and nakhlites: Inferences from chlorine-rich minerals, petrology, and geochemistry. *Meteoritics & Planetary Science* 48:819–853.
- McKay G., Mikouchi T., and Schwandt C. 2006. Additional complexities in nakhlite pyroxenes: A progress (?) report (abstract #2435). 37th Lunar and Planetary Science Conference. CD-ROM.
- McSween H. Y., Taylor G. J., and Wyatt M. B. 2009. Elemental composition of the Martian crust. *Science* 324:736–739.
- Mikouchi T., Yamada I., and Miyamoto M. 2000. Symplectic exsolution in olivine from the Nakhla Martian meteorite. *Meteoritics & Planetary Science* 35:937–942.
- Mikouchi T., Koizumi E., Monkawa A., Ueda Y., and Miyamoto M. 2003. Mineralogy and petrology of Yamato 000593: Comparison with other Martian nakhlite meteorites. *Antarctic Meteorite Research* 16:34–57.
- Mikouchi T., Miyamoto M., Koizumi E., Makishima J., and McKay G. 2006. Relative burial depths of nakhlites: An update (abstract #1865). 37th Lunar and Planetary Science Conference. CD-ROM.
- Mikouchi T., Makishima J., Kurihara T., Hoffmann V. H., and Miyamoto M. 2012. Relative burial depth of nakhlites revisited (abstract #2363). 43rd Lunar and Planetary Science Conference. CD-ROM.
- Needham A. W., Abel R. L., Tomkinson T., and Grady M. M. 2013. Martian subsurface fluid pathways and 3D mineralogy of the Nakhla meteorite. *Geochimica et Cosmochimica Acta* 116:96–110.
- Noguchi T., Nakamura T., Misawa K., Imae N., Aoki T., and Toh S. 2009. Laihunite and jarosite in the Yamato 00 nakhlites: Alteration products on Mars? *Journal of Geophysical Research* 114:E10004.
- Nyquist L. E., Bogard D. D., Shih C.-Y., Greshake A., Stöffler D., and Eugster O. 2001. Ages and geologic histories of Martian meteorites. *Space Science Review* 96:105–164.
- Owen T., Maillard J. P., de Bergh C., and Lutz B. L. 1988. Deuterium on Mars: The abundance of HDO and the value of D/H. *Science* 240:1767–1771.
- Sanborn M. E., Wadhwa M., Balta J. B., Mayne R., and McSween H. Y. 2011. Trace element geochemistry of the Nakhlite Northwest Africa 5790 (abstract). *Meteoritics & Planetary Science* 46:A203.
- Saxton J. M., Lyon I. C., and Turner G. 2000. Ion probe studies of deuterium/hydrogen in the nakhlite meteorites. *Meteoritics & Planetary Science* 35:A142–A143.
- Shih C.-Y., Nyquist L. E., Reese Y., and Jambon A. 2010. Sm-Nd isotopic studies of two nakhlites, NWA 5790 and Nakhla (abstract #1367). 41st Lunar and Planetary Science Conference. CD-ROM.
- Stopar J. D., Taylor G. J., Velbel M. A., Norman M. D., Vicenzi E. P., and Hallis L. J. 2013. Element abundances, patterns, and mobility in Nakhlite Miller Range 03346 and implications for aqueous alteration. *Geochimica et Cosmochimica Acta* 112:208–225.
- Tomkinson T., Lee M. R., Mark D. F., and Smith C. L. 2013. Sequestration of Martian CO<sub>2</sub> by mineral carbonation. *Nature Communications* 4:2662.
- Toporski J. and Steele A. 2007. Observations from a 4-year contamination study of a sample depth profile through Martian meteorite Nakhla. *Astrobiology* 7:389–401.
- Treiman A. H. 2005. The nakhlite meteorites: Augite-rich igneous rocks from Mars. *Chemie der Erde* 65:203–270.
- Treiman A. H. and Irving A. J. 2008. Petrology of Martian meteorite Northwest Africa 998. *Meteoritics & Planetary Science* 43:829–854.
- Treiman A. H. and Lindstrom D. J. 1997. Trace element geochemistry of Martian iddingsite in the Lafayette meteorite. *Journal of Geophysical Research* 102:9153–9163.
- Treiman A. H. and Steele A. 2008. Jarosite, hematite and smectite in the aqueous alteration material of the Yamato-000593/794 nakhlite (Martian meteorite). Geological Society of America Abstracts with Programs 40:6, Abstract 171–11, 208.
- Treiman A. H., Barrett R. A., and Gooding J. L. 1993. Preterrestrial aqueous alteration of the Lafayette (SNC) meteorite. *Meteoritics* 28:86–97.
- Treiman A. H., Gleason J. D., and Bogard D. D. 2000. The SNC meteorites are from Mars. *Planetary and Space Science* 48:1213–1230.
- Udry A. and McSween H. Y. 2012. Paired nakhlites MIL 090030, 090032, 090136 and 03346: New insights into the cumulate pile (abstract #1047). 43rd Lunar and Planetary Science Conference. CD-ROM.
- Usui T., Alexander C. M. O'D., Wang J. H., Simon J. I., and Jones J. H. 2012. Origin of water and mantle-crust interactions on Mars inferred from hydrogen isotopes and volatile element abundances of olivine-hosted melt inclusions of primitive shergottites. *Earth & Planetary Science Letters* 357–358:119–129.
- Velbel M. A. 2012. Aqueous alteration in Martian meteorites: Comparing mineral relations in igneous-rock weathering of Martian meteorites and in the sedimentary cycle of Mars. In *Sedimentary geology of Mars*, edited by Grotzinger J. and Milliken R. *Society for Sedimentary Geology Special Publication* 102:97–117.
- Vicenzi E. P., Tobin K., Heaney P. J., Onstott T. C., and Chun J. 1997. Carbonate in Lafayette meteorite: A detailed micro analytical study (abstract). *Meteoritics & Planetary Science* 32:A132–A133.
- Vicenzi E. P., Fries M., Fahey A., Rost D., Greenwood J. P., and Steele A. 2007. Evidence for young jarosite precipitation on Mars (abstract). *Meteoritics & Planetary Science* 42:A5293.
- Watson L. L., Hutcheon I. D., Epstein S., and Stolper E. M. 1994. Water on Mars: Clues from D/H and water contents of hydrous phases in SNC meteorites. *Science* 265:85–90.

- Weisberg M. K., Smith C. L., Benedix G., Herd C. D. K., Righter K., Haack H., Yamaguchi A., Chennaoui A. H., and Grossman J. N. 2010. The Meteoritical Bulletin, No. 97. *Meteoritics & Planetary Science* 45:449–493.
- Wlotzka F. 1993. A weathering scale for the ordinary chondrites. *Meteoritics* 28:460.

### SUPPORTING INFORMATION

Additional supporting information may be found in the online version of this article:

**Table S1:** Chemical composition of NWA 5790.

**Table S2:** Chemical composition of NWA 5790 olivine grains.

---